Case Studies in Thermal Engineering 71 (2025) 106143

Contents lists available at ScienceDirect

Case Studies in Thermal Engineering

journal homepage: www.elsevier.com/locate/csite

Simulation of conjugate free convection heat transfer of NEPCM/Al_2O_3-kerosene non-Newtonian hybrid nanoliquid between a double-pipe space

Mohamed Bouzidi [a], Hakim S. Sultan Aljibori [b], Zehba Raizah [c], Mohammed Hasan Ali [d], Taoufik Saidani [e,***], Faisal Alresheedi [f], Ahmed Elhassanein [g], Mahmoud Sabour [h,*], Mohammad Ghalambaz [i,**]

[a] Department of Physics, College of Science, University of Ha'il, Ha'il P.O. Box 2440, Saudi Arabia
[b] College of Engineering, University of Warith Al-Anbiyaa, Karbala, 56001, Iraq
[c] Department of Mathematics, Faculty of Science, King Khalid University, Abha, Saudi Arabia
[d] College of Technical Engineering, Imam Ja'afar Al-Sadiq University, Al-Muthanna, 66002, Iraq
[e] Center for Scientific Research and Entrepreneurship, Northern Border University, 73213, Arar, Saudi Arabia
[f] Department of Physics, College of Science, Qassim University, Buraidah, 51452, Saudi Arabia
[g] Department of Mathematics, College of Science, University of Bisha, P.O. Box 551, Bisha, 61922, Saudi Arabia
[h] Artificial intelligence and simulations research group, SimoAI OU, Tallinn, 10117, Estonia
[i] Department of Mathematical Sciences, Saveetha School of Engineering, SIMATS, Chennai, India

ARTICLE INFO

Keywords:
Non-Newtonian hybrid nanoliquid
Carreau model
Finite element formulation
Phase change material
Double pipes space

ABSTRACT

The current study addresses the assessment of heat and mass transfer of NEPCM/Al2O3- Kerosene hybrid nanofluid inside a double pipes space as a part of a heat exchanger. The mentioned synthesis can reflect Newtonian or non-Newtonian properties following the well-known Carreau model. After finding the governing equations including fluid flow continuity, momentum components, and thermal in the fluid and the solid parts, they have been turned into their non-dimensional form. Next, the equations were formulated based on Galerkin finite element method. The results have been configured in the forms of curves, contours, and streamlines. The Nusselt number has a determinative role in the current study as well. The findings express that the non-Newtonian hybrid nanoliquid by shear thinning property takes the lead in Nusselt number, about 42 % against the Newtonian synthesis. Instead, a deterioration in the heat transfer rate by 9 % against the Newtonian fluid is obtained via shear thickening hybrid nanoliquid. Increasing the nanoparticles volume fraction (NEPCM and Al_2O_3), has the greatest effect on the shear-thickening hybrid nanoliquid, enhancing it by 13.5 %. In contrast, the shear-thinning hybrid nanoliquid shows only a 7.5 % improvement, demonstrating the lowest sensitivity to the added nanoparticles when compared to the Newtonian and shear-thickening fluids.

* Corresponding author.
** Corresponding author.
*** Corresponding author.
E-mail addresses: elbouzidimed16@yahoo.com (M. Bouzidi), hakim.s@uowa.edu.iq (H.S. Sultan Aljibori), zaalrazh@kku.edu.sa (Z. Raizah), mohammed.hasan@sadiq.edu.iq (M.H. Ali), Taoufik.Saidan@nbu.edu.sa (T. Saidani), f.alresheedi@qu.edu.sa (F. Alresheedi), el_hassanein@yahoo.com (A. Elhassanein), m.sabour1990@gmail.com (M. Sabour), m.ghalambaz@gmail.com (M. Ghalambaz).

https://doi.org/10.1016/j.csite.2025.106143
Received 12 December 2024; Received in revised form 7 March 2025; Accepted 13 April 2025
Available online 15 April 2025

Nomenclature

Latin letters	
Cp	Constant pressure specific heat (J/kg K)
Cr	Ratio of heat capacity
d	Inner pipe diameter (*m*)
D	Outer pipe diameter (*m*)
f	Scaled fusion function defined by Eq. (21)
g	Gravity (m/s^2)
h	Thermal convective coefficient (W/m^2 K)
k	Thermal conductivity coefficient (W/m K)
Nu	Nusselt number
p	Pressure (Pa)
P	Scaled pressure
Pr	Prandtl number
Ra	Rayleigh number
S	Interface surface (*m*)
Ste	Stefan number
t	Thickness of inner pipe (*m*)
T	Temperature (K)
u	Velocity in x- direction (m/s)
U	Scaled velocity in X-direction
v	y- velocity (m/s)
V	Scaled velocity in Y-direction
x	Horizontal Cartesian coordinate (*m*)
X	Scaled horizontal Cartesian coordinate
y	Vertical Cartesian coordinate (*m*)
Y	Scaled vertical Cartesian coordinate (*m*)
Greek symbols	
α	Thermal diffusivity (m^2/s)
β	Thermal expansion coefficient (1/K)
δ	Dimensionless parameter of fusion range
μ	Dynamic viscosity (Pa.s)
θ	Dimensionless temperature
λ	The heat capacity ratio of the NEPCM nanoparticles to the host fluid
ρ	Density (kg/m^3)
φ	Nanoparticles concentration (simple and NECPM particles)
ψ	Stream function
Subscript	
b	Suspension Bulk properties
C	Cold wall
f	Fusion property
H	Hot wall
hnl	Hybrid nanoliquid
Host	Base fluid
L	Local
mean	mean value of Nusselt number
NEPCM	Nano- Encapsulated phase change materials particles.
SNP	Simple nanoparticles

1. Introduction

Non-Newtonian fluids, characterized by their viscosity dependency on shear rate, exhibit distinct behaviors compared to Newtonian fluids in heat transfer processes. These types of fluids may behave as Shear thinning (Pseudoplastic) or shear thickening (Dilatant) ones. Hence, based on type of the non-Newtonian fluids, their applications can be categorized. Generally, in the present field, the mentioned fluids can be utilized in the different types of heat exchangers [1,2], reactors [3], natural polymer [4], and damping applications [5]. A comprehensive review of recent literature highlights significant findings regarding the impact of non-Newtonian suspensions on heat and mass transfer.

In a numerical investigation, Pishkar et al. [6] probed the non-Newtonian fluid behavior impression on free convection heat transfer in the cavities. According to their findings [6], Pseudoplastic fluids enhance heat transfer rate due to reduced dynamic viscosity through an augmented shear rate, whereas dilatant fluids exhibit lower heat transfer rates since the dynamic viscosity is augmented. In their numerical investigation, Yazdani et al. [7] assessed the impact of entropy generation and free convection inside a porous trapezoidal cavity saturated by a power-law non-Newtonian fluid. The research applied a continuum approach to simulate fluid movement in the porous environment, adjusting Darcy's formula to reflect the unique rheological properties of the non-Newtonian fluid. The results [7] indicated that the power-law index significantly influences both the heat transfer rate and entropy generation, especially under prevailing convection conditions in the enclosure. The influence was notably stronger when the fluids showed the shear thinning behavior. Jahanbakhshi et al. [8] evaluated the magnetic field impression on non-Newtonian fluid flow, revealing contrasting heat transfer behaviors for shear-thinning and shear-thickening fluids compared to Newtonian ones. Moreover, Roy et al. [9] analyzed forced, free, and mixed convection scenarios in a quadrilateral enclosure, demonstrating that higher power-law indices correspond to greater heat transfer rate. They [9] identified the optimal heat transfer medium for different convection modes,

contributing to cost-effective design strategies. Loenko and Sheremet [10] addressed pseudoplastic non-Newtonian effects in a cavity with heat generation using a finite different approach. A numerical investigation on a dilatant non- Newtonian liquid in the laminar natural convection regime between two concentric cylinders has been conducted by Benhizia and Bouzit [11]. They emphasized that dilatant fluids exhibit solid-like behavior rather than typical fluid behavior, influencing heat transfer mechanisms. Specifically, the Rayleigh number was found to enhance convective flow, resulting in an increased Nusselt number. Other aspects of heat transfer in cavities such as double-diffusive convection [12], Darcy terms [13], magnetohydrodynamics [14], wall boundaries [14], and mixed convection effects [15] have been investigated in recent studies.

Sometimes, the thermal performance of the Newtonian/non-Newtonian fluid which is used as a working one, cannot have a suitable performance. As a common rule in the field, well-known nanoparticles of different types, shapes, and sizes are added to a pure non-Newtonian fluid to make an effective change in the equipment's thermal performance. Majeed et al. [16] considered a wavy enclosure and assessed nanoliquids' heat transfer rate in the presence of a uniform magnetic field. As a non-dimensional result, increasing Hartmann's number reduces both heat transfer rate and nanoliquid velocity. Tasmin et al. [17], explored heat transfer and thermodynamic second law-based entropy generation in non-Newtonian nanoliquid flowing within wavy porous cavities. They [17] highlighted the significance of power-law effects on Nusselt number increment, particularly in high Darcy–Rayleigh number regimes. The wavy cavity geometry profoundly influences flow patterns and entropy generation rates, showcasing the complexity of non-Newtonian fluid behaviors in intricate geometries. As an experimental work, Hojjat et al. [18], focused on the non-Newtonian nanoliquids inside circular tubes. Forced convection mode was dominant in the mentioned tubes. They [18] observed that the addition of nanoparticles, such as Al_2O_3, CuO, and TiO_2, into carboxymethyl cellulose (CMC) base fluids, causes heat transfer coefficients to get better. The heat transfer rate enhancement was found to get better via nanoparticle concentration. The non-Newtonian nanoliquids, as heat transfer ones, within a helical baffle heat exchanger were explored by Tan et al. [19]. According to their experiments [19], Xanthan Gum (XG) solutions included a specific volume fraction of multi-walled carbon nanotubes (MWCNTs). The results showed significant improvements in convective heat transfer coefficients against the pure fluid. In addition, the increment is augmented with both of Peclet number and nanoparticles volume fraction.

Abderrahmane et al. [20] studied convective non-Newtonian nanoliquids within a slanted half-annulus enclosure. Their research [20] illustrated that integrating Al_2O_3 nanoparticles into a water-based fluid, which displays shear-thinning properties, led to a reduced heat transfer rate due to the presence of a consistent magnetic field traversing the enclosure. Additionally, an increase in the power-law index corresponded to a reduction in the Nusselt number. In related work, Naik and Vinod [21] explored shell and helical coil heat exchangers using non-Newtonian nano-fluids experimentally. They observed [21] that both the nanoparticles concentration and the temperature of the fluid on the shell side enhanced the heat transfer coefficients. A further study by Naik and Vinod [22] assessed the impression of various species of nanoparticles on the thermal performance of non-Newtonian carboxymethyl cellulose (CMC) fluids in shell and helical coil heat exchangers. In this experiment [22], they dispersed nanoparticles such as Al_2O_3, Fe_2O_3, and CuO in an aqueous CMC solution. Their findings highlighted that CuO nanoparticles achieved the highest increase in temperature, attributed to their superior thermal conductivity.

Anitha and Pichumani [23] conducted a numerical evaluation of thermal efficacy in industrial double-pipe heat exchangers employing nano-fluids composed of CNTs in both Newtonian and non-Newtonian forms. Their observations [23] indicated marked enhancements in thermal performance when a mixture of Newtonian and non-Newtonian nano-fluids was utilized. Moreover, overall heat transfer coefficients had an increment of 25 %. Vallabh and Ghoshdastidar [24] analyzed the heat transfer characteristics within a quadrilateral cavity using both mixed Newtonian/non-Newtonian nano-fluids and solely non-Newtonian nano-fluids. Their findings [24] indicated that incorporating a higher proportion of Alumina nanoparticles enhanced Nusselt number in mixed nano-fluids until reaching a threshold nanoparticle volume fraction, after which the heat transfer rate declined.

In a separate study, Maleki et al. [25] evaluated the heat and mass transfer properties of non-Newtonian nanoliquids across porous media. They discovered that the type of nanoparticles and the application of either injection or suction had a substantial impact on the heat transfer efficiency. Notably, non-Newtonian nanoliquids demonstrated enhanced heat transfer compared to Newtonian nano-fluids under conditions involving suction and an impermeable surface, although the nanoparticle type had a greater impact within suction scenarios.

Meanwhile, Shahsavar et al. [26] explored enhancements in a double-pipe heat exchanger (DPHE) by integrating twisted tubes with non-Newtonian nanoliquids. Their simulations of laminar flow with non-Newtonian CuO nanoliquids in the DPHE showed that the combined use of twisted tubes and nanoliquids significantly improved both heat transfer and overall thermal efficiency.

When focusing on enhancing the heat transfer rate associated with the absorption, storage, and release of thermal energy, the integration of nano-encapsulated phase change materials (NEPCMs) into a host fluid, whether Newtonian or non-Newtonian, proves beneficial. NEPCMs, comprising a core and a shell structure, inherently possess a high specific heat capacity. The phase change occurs within the core, while the solid shell acts to contain the core effectively, similar to a container. Phase change process of hybrid nano-PCM, molten salt- Molybdenum disulfide- Iron oxide, inside a thermal energy storage (TES), has been simulated by Waqas et al. [27]. They [27] utilized various numbers and arrangements of leaf-shaped fins which are placed in the referred TES. The evaluations have been provided against the pure molten salt. The results revealed that a greater percentage of both nanoparticles can increase the heat transfer rate; consequently, reducing the time of melting process. Moreover, the fins with leaf-vein shape augment liquid fraction in the storage tank, dramatically. Using ordinary differential equations, the melting process of Water- Copper/Alumina hybrid nanofluid over a stretching disk has been demonstrated [28]. The authors [28] considered Bodewadt boundary layer flow and magnetohydrodynamic (MHD) impression over the mentioned disk. Better temperature distribution and heat transfer rate through increasing melting temperature and nanoparticle volume fraction could be the most prominent results obtained in the reviewed study, respectively. In another study, Waqas et al. [29] demonstrated some curve-shaped fins in a TES system and investigated the melting process of the

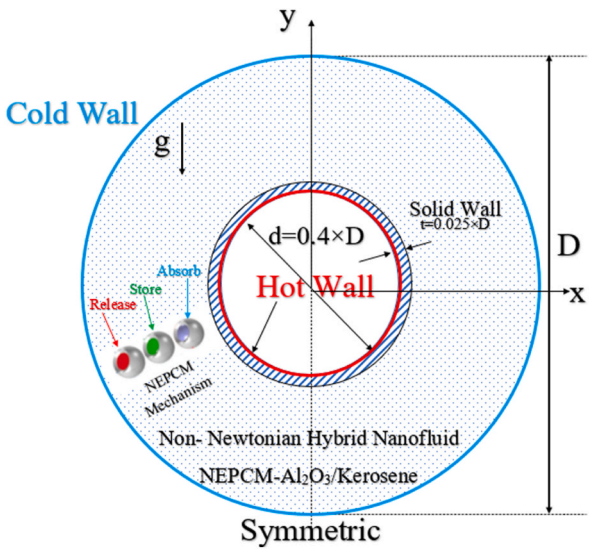

Fig. 1. A scheme of the physical model proposed in the current study. The enclosure is filled by NEPCM- Al_2O_3/Kerosene hybrid nanoliquid.

nano-PCMs, molten salt- Alumina, and molten salt MWCNTs. Indeed, the enhancement of TES efficiency via both fins and nano-PCM was the purpose of the authors. The results showed that the introduced approaches can create significant effects on the melting time. As a numerical study, Ali et al. [30] simulated the convection of non-Newtonian fluids containing NEPCM suspensions within a quadrilateral enclosure, employing the power-law method to assess the behavior of the synthesized mixture. Their analysis revealed that the NEPCM fusion temperature significantly affects the heat transfer rate. Furthermore, they noted a linear enhancement in heat transfer rate correlated with specified power-law index values, particularly under conditions where the non-Newtonian nanoliquid exhibited shear-thinning behavior.

Dogonchi et al. [31] undertook a study on the thermal performance and entropy production, following the second law of thermodynamics, in a non-Newtonian NEPCM fluid inside an inclined enclosure featuring an internal heater. Using numerical techniques, they explored the impacts of different parameters including the enclosure's tilt angle, the power-law index, the Rayleigh number, and the nanoparticles concentration. Their results [31] indicated that dilatant fluids, with a power-law index greater than 1, might be less suitable for heat transfer applications as increases in the power-law index led to decreased Nusselt number. Nonetheless, they observed [31] that adjusting the tilt angle of the cavity proved to be an effective strategy for optimizing heat transfer and controlling entropy production.

Recent advancements in materials science and engineering have significantly propelled the development of nanoliquids, with the field now moving toward more innovative configurations. Specifically, the incorporation of two or more distinct types of nanoparticles into a base fluid creates a hybrid nanoliquid, which exhibits superior thermal performance compared to conventional fluids. This combination of nanoparticles, each contributing unique properties such as enhanced thermal conductivity, results in a fluid with improved heat transfer capabilities. The resulting mixture is known as a hybrid nanoliquid, and its unique characteristics have opened up new possibilities for a wide range of industrial and engineering applications. Hussain et al. [32] investigated the conjugate free convection of non-Newtonian hybrid nanoliquid within a sinusoidal-shaped cavity through numerical simulations. Their findings demonstrated that pseudo-plastic hybrid nanoliquids with strong Rayleigh numbers and favorable thermal conductivity ratios achieved the highest heat transfer rates, particularly when the power-law index played a critical role at elevated Rayleigh numbers. In a numerical study, Ahmad et al. [33] evaluated the conjugate free convection heat transfer of a double-diffusive non-Newtonian liquid in an enclosure. The liquid was affected by an inclined uniform magnetic field. They [33] probed the effect of non-dimensional numbers and parameters on the entropy generation. It was found that the entropy arising from the magnetic field has a trivial impression in the solid parts, while the other terms of the entropy generation have the maximum portion in the same parts. Batool and Nawaz [34] conducted a study on thermal performance using non-Newtonian fluids containing hybrid microstructures in a cavity. They introduced CuO and Al2O3 nanoparticles into fluids characterized by micro-inertia and vortex viscosity effects, noting a marked increase in thermal performance due to the hybrid microstructure components.

Further, Bahiraei et al. [35] examined the heat and mass transfer properties of a non-Newtonian hybrid nanoliquid in a double-pipe minichannel heat exchanger. Their hybrid nanoliquid, composed of TMAH-coated Fe_3O_4 nanoparticles and GA-coated CNTs, significantly outperformed H_2O in terms of heat transfer rates. Nadooshan et al. [36] assessed the rheological treatment of Fe_3O_4-MWCNTs/ethylene glycol hybrid nanoliquid, observing that it displayed Newtonian and non-Newtonian behavior at lower and higher nanoparticle volume fractions, respectively, affecting the heat transfer efficiency. Lastly, Shahsavar and Bahiraei [37] explored the thermal conductivity and dynamic viscosity of a non-Newtonian hybrid nanoliquid that includes Fe_3O_4 nanoparticles and CNTs. They [27] extended and validated Artificial Neural Network (ANN) schemes to forecast these properties, which showed a strong correlation with experimental outcomes.

Table 1
The thermophysical characteristics of NEPCM (core and shell), Kerosene host fluid, and Al_2O_3 nanoparticles, as cited from Refs. [41–45].

Material	ρ (kg/m^3)	k (W/m.K)	β (K^{-1})	C_p (J/kg.K)
Nonadecane (NEPCMs core)	721	–	–	2037
Polyurethane (NEPCMs Shell)	786	0.05	17.28×10^{-5}	1317.7
Host fluid (Kerosene)	790	0.101	10×10^{-4}	2010
Al_2O_3	3950	40	17.4×10^{-6}	773

Bahiraei et al. [38] investigated irreversibility using a non-Newtonian hybrid nanoliquid in a double-tube minichannel. Their results indicated that at lower nanoparticle volume fractions, the heat transfer component outweighed entropy production, whereas at higher concentrations, friction became the dominant contributor to entropy production. Alnaqi et al. [39] studied the effects of irreversibility in non-Newtonian MWCNTs-SiO2/EG-H2O hybrid nanoliquids inside a zigzag microchannel heat sink. They noted that both increased nanoparticle concentration and greater zigzag heights enhanced heat transfer but also led to increased entropy generation. In a similar vein, Dawar et al. [40] explored the thermal behavior of a non-Newtonian tangent hyperbolic hybrid nanoliquid as it flowed over a non-isothermal flat plate. Their findings revealed that higher concentrations of ferrous and graphene oxide nanoparticles negatively affected the velocity fields but improved the thermal fields, a result attributed to variations in dynamic viscosity and relaxation times.

The current study focuses on the conjugate free convection heat transfer of NEPCM/Al_2O_3- Kerosene as a Newtonian and non-Newtonian hybrid nanoliquid inside a double pipe space. According to the reviewed papers, none of them has covered all the suggested options which are provided by the present study.

2. Model description and governing equations

2.1. Model description

A double pipe space as a part of a shell and tube heat exchanger is depicted in Fig. 1. The inner pipe with the specified thickness gets hot through a fluid that flows within the pipe, while, the outer pipe is here for cooling down the inner one. The space between the pipes is saturated by NEPCM- Al_2O_3/Kerosene hybrid nanoliquid. It can reflect non-Newtonian behavior based on the Carreau model. The Carreau model is chosen here because it offers a greater degree of flexibility and a more realistic representation of fluid behavior compared to the Power-Law model. Specifically, the Carreau model captures shear-thinning and shear-thickening behaviors more accurately, which is critical when studying the complex rheological properties of NEPC nanoliquids. Furthermore, the Carreau model allows for a smoother transition between the Newtonian and non-Newtonian regimes, which is important for accurately reflecting the varying flow conditions under different shear rates. This makes it a more suitable choice for modeling the flow of hybrid nanoliquids in the current study.

The dispersed NEPCM particles absorb heat close to the hot inner pipe, store it in the middle areas, and release the gained energy near the cold outer pipe. On the other hand, Al_2O_3 nanoparticles have been suspended in Kerosene host fluid to utilize their potential properties in the heat transfer process. According to the descriptions, conjugate free convection is dominant in the area placed between the double pipes space. So, the buoyancy forces will have a key role regarding the fluid flow circulation. To do it, valid Boussinesq's approximation is current in the mentioned area; where, obtaining the symmetric patterns for the heat and fluid flow can be expected on the vertical axis. It is worth noting that any slip velocity condition between the pipe surface and non-Newtonian hybrid nanoliquid would be ignored.

As noted, nano-encapsulated phase change materials (NEPCM), and Alumina nanoparticles with a determined volume fraction have been dispersed inside Kerosene host fluid. Their thermophysical properties have been determined in Table 1. Based on the collected data in this table, the specific heat capacity value of the NEPCM is high. On the other hand, Alumina nanoparticles have a superior thermal conductivity against Kerosene host fluid and the NEPCMs. Thus, a fully augmented synthesis than each one of regular nanoliquids, Kerosene- NEPCM and or Kerosene- Al_2O_3, can be expected.

2.2. Governing equations

As referred to in the model description subsection, the obtained suspension shows a non-Newtonian behavior following the Carreau model. In the such models, dynamic viscosity would be a non-linear function of the shear rate. To this purpose, the dynamic viscosity of the non-Newtonian hybrid nanoliquid ($\mu_{hnl}(\gamma^*)$) can be assigned as follows [46,47]:

$$\frac{\mu_{hnl}(\gamma^*)-\mu_\infty}{\mu_{hnl}-\mu_\infty}=\left(1+(\lambda^*\gamma^*)^2\right)^{\frac{n-1}{2}} \tag{1}$$

in addition, it is supposed that $\mu_\infty \ll \mu_{hnl}$, hence, Equation (1) is diminished to:

$$\mu_{hnl}(\gamma^*)=\mu_{hnl}\left(1+(\lambda^*\gamma^*)^2\right)^{\frac{n-1}{2}}, \tag{2}$$

in the above equation, the dimensional shear rate can be written as below:

$$\gamma^* = \max\left(\sqrt{[D'] : [D']}, \gamma^*_{\min}\right), D' = \frac{1}{2}\left(u^{*2} + v^{*2}\right) \tag{3}$$

D', shows shear rate tensor as a function of squared velocity components.

also, μ_{hnl}, λ^*, and μ_∞, are defined as the initial value of non-Newtonian hybrid nanoliquid dynamic viscosity, time-dependent term in the Carreau model, and dynamic viscosity of the ambient, respectively. Carreau index for non- Newtonian hybrid nanoliquid, is shown via n symbol. On the one hand, when $n < 1$, the non-Newtonian suspension behaves as a pseudoplastic fluid, a shear-thinning one. On the other hand, $n > 1$ means that the non-Newtonian suspension transforms into a Dilatant fluid, well-known as a shear thickening one. Inevitably, $n = 1$, adds up to the familiar Newtonian suspension.

Taking into account equation (2), the governing equations containing fluid flow continuity, momentum components, and, the energy of the non-Newtonian hybrid nanoliquid as well as energy in the solid wall (inner pipe with determined thickness), have been shown in equations (4)–(8) [48–50]:

continuity

$$\frac{\partial u^*}{\partial x^*} + \frac{\partial v^*}{\partial y^*} = 0 \tag{4}$$

2.2.1. Momentum components

$$\rho_{hnl}\left(u^*\frac{\partial u^*}{\partial x^*} + v^*\frac{\partial u^*}{\partial y^*}\right) = -\frac{\partial p^*}{\partial x^*} + \mu_{hnl}\left(\frac{\partial^2 u^*}{\partial x^{*2}} + \frac{\partial^2 u^*}{\partial y^{*2}}\right)\left(1 + (\lambda^*\gamma^*)^2\right)^{\frac{n-1}{2}} \tag{5}$$

$$\rho_{hnl}\left(u^*\frac{\partial v^*}{\partial x^*} + v^*\frac{\partial v^*}{\partial y^*}\right) = -\frac{\partial p^*}{\partial y^*} + \mu_{hnl}\left(\frac{\partial^2 v^*}{\partial x^{*2}} + \frac{\partial^2 v^*}{\partial y^{*2}}\right)\left(1 + (\lambda^*\gamma^*)^2\right)^{\frac{n-1}{2}} + g\rho_{hnl}\beta_{hnl}(T - T_c) \tag{6}$$

energy (thermal) equation in non- Newtonian hybrid nanoliquid

$$(\rho C_p)_{hnl}\left(u^*\frac{\partial T}{\partial x^*} + v^*\frac{\partial T}{\partial y^*}\right) = k_{hnl}\left(\frac{\partial^2 T}{\partial x^{*2}} + \frac{\partial^2 T}{\partial y^{*2}}\right) \tag{7}$$

As mentioned, the inner pipe has a specified thickness; So, thermal equation in the body of inner pipe can be written as

$$k_s\left(\frac{\partial^2 T}{\partial x^{*2}} + \frac{\partial^2 T}{\partial y^{*2}}\right) = 0 \tag{8}$$

In the above equations, ρ_{hnl} and $C_{p,hnl}$ define the density and specific heat capacity of the non-Newtonian hybrid nanoliquid, respectively. β_{hnl} is thermal expansion coefficient and k_{hnl}, symbolizes the thermal conductivity of the mentioned suspension.

The set of Equation (9) builds up the boundary conditions regarding the suggested physical model in Fig. 1:

$T = T_h, u^* = v^* = 0$ On the inner diameter of the inner pipe (9-a)

$k_s\frac{\partial T}{\partial n}\Big|_s = k_b\frac{\partial T}{\partial n}\Big|_b, u^* = v^* = 0$ On the outer diameter of the inner pipe (9-b)

$T = T_c, u^* = v^* = 0$ On the outer pipe (9-c)

2.3. Physical properties

By introducing equation (10), and (11), the density, ρ_{hnl}, and the heat capacity, $(\rho C_p)_{hnl}$ for the introduced suspension are [51]:

$$\rho_{hnl} = \varphi_{NEPCM}\rho_{NEPCM} + \varphi_{SNP}\rho_{SNP} + (1 - \varphi_{hnl})\rho_{host} \tag{10}$$

$$(\rho C_p)_{hnl} = \varphi_{NEPCM}(\rho C_p)_{NEPCM} + \varphi_{SNP}(\rho C_p)_{SNP} + (1 - \varphi_{hnl})(\rho C_p)_{host} \tag{11}$$

Equation (12) has been assigned to the thermal expansion coefficient of the non-Newtonian hybrid nanoliquid, β_{hnl}:

$$\beta_{hnl} = \varphi_{NEPCM}\beta_{NEPCM} + \varphi_{SNP}\beta_{SNP} + (1 - \varphi_{hnl})\beta_{host} \tag{12}$$

and, $\frac{\beta_{hnl}}{\beta_{host}}$ ratio can be specified as:

$$\frac{\beta_{hnl}}{\beta_{host}} = \varphi_{NEPCM}\frac{\beta_{NEPCM}}{\beta_{host}} + \varphi_{SNP}\frac{\beta_{SNP}}{\beta_{host}} + (1 - \varphi_{hnl}) \tag{13}$$

thermal expansion of the nanoparticles (β_{SNP} and β_{NEPCM}) has a very small value against that of the host fluid (β_{host}); thus, $\frac{\beta_{NEPCM}}{\beta_{host}} \longrightarrow 0$, and

$\frac{\beta_{SNP}}{\beta_{host}} \rightarrow 0$ in equation (13). Consequently, Equation (13) is declined to the below form:

$$\frac{\beta_{hnl}}{\beta_{host}} = (1 - \varphi_{hnl}) \tag{14}$$

Moreover, an expression of non-Newtonian dynamic viscosity ratio (μ_r), can be expressed as below:

$$\mu_r = \frac{\mu_{hnl}(\gamma^*)}{\mu_{host}} = \frac{\mu_{hnl}}{\mu_{host}}\left(1 + (\lambda\gamma)^2\right)^{\frac{n-1}{2}}, \tag{15}$$

in equation (15), λ, and γ show the dimensionless scheme of the shear rate and time-dependent parameter. Importantly, there is a reverse dimensional relation between the shear rate $\left[\frac{1}{s}\right]$, and time-dependent parameter $[s]$, causing both of them to be dimensionless, automatically.

The dynamic viscosity of the hybrid nanoliquid as a part of the non-Newtonian dynamic viscosity ratio (μ_r), is established for upgraded Brinkmann equation [52]:

$$\frac{\mu_{hnl}}{\mu_{host}} = \frac{1}{(1 - \varphi_{SNP} - \varphi_{NEPCM})^{2.5}} \tag{16}$$

Regarding the hybrid nanoliquid thermal conductivity, the following relation, raised of Maxwell equation is provided [52]:

$$\frac{k_{hnl}}{k_{host}} = \frac{\frac{(\varphi_{SNP}k_{SNP} + \varphi_{NEPCM}k_{NEPCM})}{\varphi_{hnl}} + 2k_{bf} + 2(\varphi_{SNP}k_{SNP} + \varphi_{NEPCM}k_{NEPCM}) - 2\varphi_{hnl}k_{bf}}{\frac{(\varphi_{SNP}k_{SNP} + \varphi_{NEPCM}k_{NEPCM})}{\varphi_{hnl}} + 2k_{bf} - 2(\varphi_{SNP}k_{SNP} + \varphi_{NEPCM}k_{NEPCM}) - 2\varphi_{hnl}k_{bf}} \tag{17}$$

where, $\varphi_{hnl} = \varphi_{SNP} + \varphi_{NEPCM}$. subscripts "*SNP*", and "*NEPCM*" belong to simple nanoparticles (Al_2O_3) which do have not any phase change process, and nano-encapsulated phase change materials (polyurethane shell and nonadecane core), respectively.

2.4. Scaled equations

To create the standard results, the governing equations and the corresponding boundary conditions are transformed into their dimensionless form. Hence, Equation (18) have been taken part in the governing equations (4)–(8):

$$(\mathrm{x}, \mathrm{y}) = \frac{(x^*, y^*)}{D}, \mathrm{u} = \frac{u^* D}{\alpha_{host}}, v = \frac{v^* D}{\alpha_{host}}, p = \frac{p^* D^2}{\rho_{host}\alpha_{host}^2}, \theta = \frac{T - T_c}{T_h - T_c}, \theta_m = \frac{T_m - T_c}{(T_h - T_c)} \tag{18}$$

applying the above equations, governing equations (4)–(8) are presented in the dimensionless form:

$$\frac{\partial u}{\partial x} + \frac{\partial v}{\partial y} = 0 \tag{19}$$

$$\frac{\rho_{hnl}}{\rho_{host}}\left(u\frac{\partial u}{\partial x} + v\frac{\partial u}{\partial y}\right) = -\frac{\partial p}{\partial x} + \mu_r\, Pr\left(\frac{\partial^2 u}{\partial x^2} + \frac{\partial^2 u}{\partial y^2}\right) \tag{20}$$

$$\frac{\rho_{hnl}}{\rho_{host}}\left(u\frac{\partial v}{\partial x} + v\frac{\partial v}{\partial y}\right) = -\frac{\partial p}{\partial y} + \mu_r\, Pr\left(\frac{\partial^2 v}{\partial x^2} + \frac{\partial^2 v}{\partial y^2}\right) + \frac{(\rho\beta)_{hnf}}{(\rho\beta)_{host}} Ra\, Pr\, \theta \tag{21}$$

$$\frac{(\rho C_p)_{hnl}}{(\rho C_p)_{host}}\left(u\frac{\partial \theta}{\partial x} + v\frac{\partial \theta}{\partial y}\right) = \frac{k_{hnl}}{k_{host}}\left(\frac{\partial^2 \theta}{\partial x^2} + \frac{\partial^2 \theta}{\partial y^2}\right) \tag{22}$$

$$R_k\left(\frac{\partial^2 \theta}{\partial x^2} + \frac{\partial^2 \theta}{\partial y^2}\right) = 0, R_k = \frac{k_s}{k_{host}} \tag{23}$$

Ra, and Pr symbols which are appeared in Equation (20), and (21), define Rayleigh and Prandtl numbers, respectively. Equation (24) shows the mathematical description of each one:

$$Ra = \frac{g\rho_{host}\beta_{host}\Delta T L^3}{\alpha_{host}\mu_{host}}, Pr = \frac{\mu_{host}}{\rho_{host}\alpha_{host}} \tag{24}$$

in equation (22),

$$Cr = \frac{(\rho C_p)_{hnl}}{(\rho C_p)_{host}} = (1 - \varphi_{hnl}) + \varphi_{SNP}\Upsilon_{SNP} + \varphi_{NEPCM}\Upsilon_{NEPCM} + \frac{\varphi_{NEPCM}}{\delta\, Ste} f \tag{25}$$

Cr shows the heat capacity of NEPCM/Al2O3-Kerosene non-Newtonian Hybrid nanoliquid against the sensible heat capacity of the

Table 2
Impression of mesh size on mean Nusselt number for $Ra = 10^5$, $Pr = 28.1$, $R_k = 100$, $Ste = 0.3$, $\chi_0 = 10^{-4}$, $\varphi_{hnf} = 0.05$ ($\varphi_{NEPCM} = 0.025$, $\varphi_{SNP} = 0.025$), $\theta_f = 0.3$, and $n = 0.65$.

Case No.	Mesh quality	Mesh quantity (Overall number of Elements)	Nu_{mean}	$\lvert Err(\%)\rvert$
1	Normal	2226	7.8125	1.4
2	Fine	3384	7.9232	0.71
3	Finer	9528	7.8675	0.09
4	**Extra Fine**	**24800**	**7.8749**	**0.02**
5	Extremely fine	35944	7.8765	–

*The chosen gird size has been identified in Bold style.

Kerosene host fluid. In addition, there have been some variables in Equation (25) that are described in Equation (26), mathematically. Υ shows both of heat capacity ratio for simple nanoparticles (SNP) and nano-encapsulated phase change materials (NEPCM). δ symbol provides the dimensionless phase transition range and finally, *Ste* represents Stefan number.

$$\Upsilon_{SNP} = \left(\frac{(\rho C_p)_{SNP}}{(\rho C_p)_{host}}\right), \Upsilon_{NEPCM} = \frac{(Cp_{core,l} + \iota Cp_{shell})\rho_{core}\rho_{shell}}{(\rho Cp)_{host}(\rho_{sell} + \iota\rho_{core})}, \delta = \frac{T_{Mr}}{\Delta T},$$
$$Ste = \frac{(\rho Cp)_{host}\Delta T(\rho_{sell} + \iota\rho_{core})}{\alpha_{host}(h_{sf}\rho_{core}\rho_{sell})} \tag{26}$$

the dimensionless fusion function depicted in equation (25), f, can be defined as:

$$f = \frac{\pi}{2}\sin\left[\left(\frac{\delta}{2} + \theta - \theta_m\right)\frac{\pi}{\delta}\right] \times \begin{cases} 0 & \theta < \theta_m - \delta/2 \\ 1 & \theta_m - \delta/2 < \theta < \theta_f + \delta/2 \\ 0 & \theta > \theta_m + \delta/2 \end{cases} \tag{27}$$

also, the dimensionless fusion temperature, θ_f is:

$$\theta_f = \frac{T_m - T_c}{\Delta T} \tag{28}$$

Equations (9)–(11), the boundary conditions, are explained in the dimensionless form. The set of Equation (29) reflects them:

$$\theta = 1, u = v = 0 \text{ On the inner diameter of the inner pipe} \tag{29-a}$$

$$R_k\frac{\partial\theta_s}{\partial n} = \frac{\partial\theta}{\partial n} \text{ On the outer diameter of the inner pipe} \tag{29-b}$$

$$\theta = 0, u = v = 0 \text{ On the outer pipe} \tag{29-c}$$

furthermore, the streamline function in its dimensionless form (ω) can be obtained as:

$$\nabla^2\omega = \left(\frac{\partial U}{\partial Y} - \frac{\partial V}{\partial X}\right) \tag{30}$$

where $U = \partial\omega/\partial Y$, and $V = -\partial\omega/\partial X$. As an important note, $\omega = 0$ was considered on the pipe surface as mentioned in Refs. [53,54].

2.5. Parameters of interest

As the most widely recognized quantitative criterion in heat transfer analysis, the non-dimensional Nusselt number is considered in this study. To facilitate a meaningful discussion, the Nusselt number is specifically evaluated at the outer surface of the inner pipe, referred to as the interface surface:

$$Nu_{\text{Local}} = -\frac{k_{hnl}}{k_{host}}\left(\frac{\partial\theta}{\partial n}\right)_{\text{on interface surface}} \tag{31}$$

additionally, the mean Nusselt number on the interface surface can be obtained through the integral of equation (35):

$$Nu_{\text{Mean}} = \int -\frac{k_{hnl}}{k_{host}}\left(\frac{\partial\theta}{\partial n}\right)_{\text{on interface surface}} dn \tag{32}$$

3. Numerical approach and grid sensitivity analysis

The governing equations for fluid flow continuity, momentum, and energy (thermal) in both the fluid and solid walls are expressed as partial differential equations. These are then transformed into their dimensionless form according to the given boundary conditions

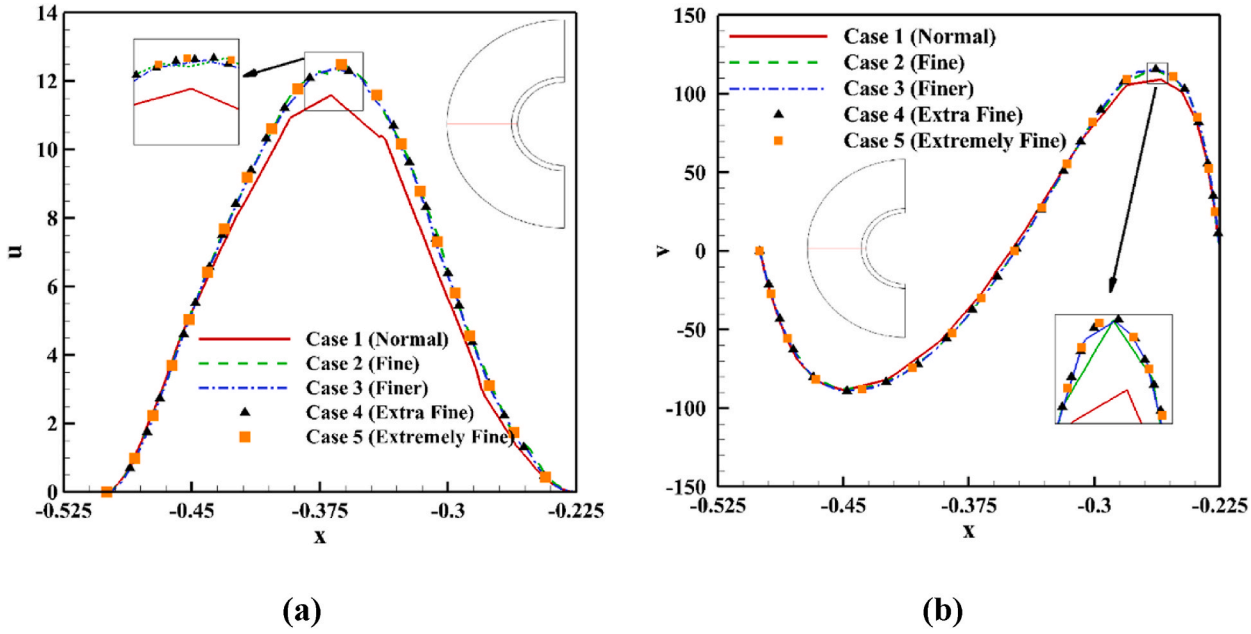

Fig. 2. (a) Horizontal component of velocity and (b) vertical component of velocity, at mid-plane of the double pipes space at $Y = 0$ for different assessed grid sizes.

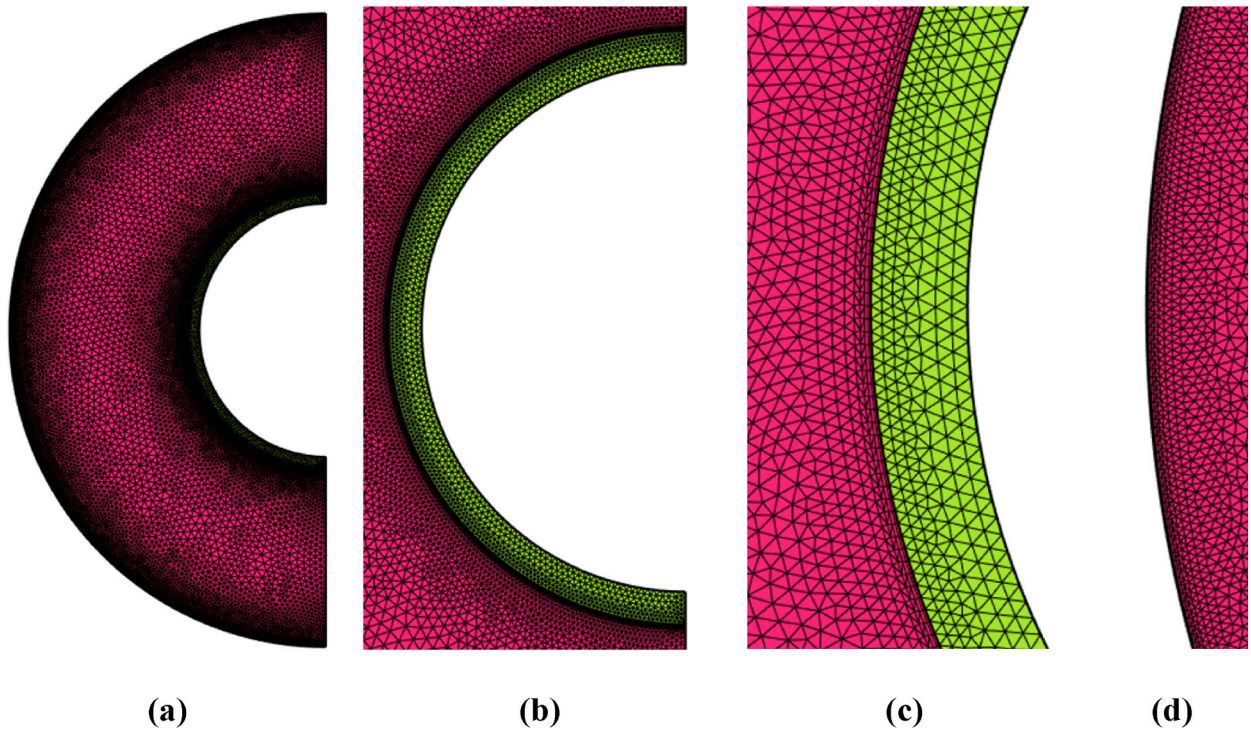

Fig. 3. Probing the chosen grid size; (a) whole of the physical model, (b) Close to inner pipe, (c) Elements in the body of the inner pipe, and (d) Close to the outer pipe.

and incorporated into the finite element scheme. To accomplish this, the Galerkin finite element method (GFEM) is used. This method ensures consistency between the trial and test functions. The trial function approximates the solution, while the test function is used to multiply the residuals, resulting in the weak (integral) form of the equations. The reason for choosing GFEM in this study, as opposed to other methods, is that it uses an equal number of trial and test functions, providing an advantage over alternative approaches.

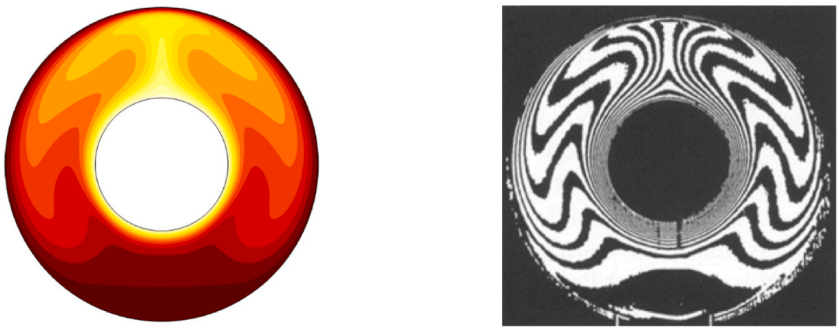

(a) (b)

Fig. 4. (Left side) The result obtained through current code versus (right side) that of provided by Guj et al. [58] in $Ra = 82700$.

Fig. 5. The obtained streamlines through the current code (black lines) and the data reported in Ghalambaz et al. [52] (brrown lines). (For interpretation of the references to colour in this figure legend, the reader is referred to the Web version of this article.)

Specifically, GFEM simplifies the solution of such problems. The weak form of the partial differential equations is derived by integrating the product of the trial function and the residual.

The field variables in the dimensionless form, (θ, u and v) are discretized in accordance to $\{\xi\}_{k=1}^{N}$ series in the range of $0.4 \leq x \leq 1$, and $0.4 \leq y \leq 1$ [55]. The fully coupled governing equations are solved through the Newton method within an iterative progress. The iterations were continued until the related non-linear residual reached an error below 10^{-6}. Extra information about the employed numerical method has been explained in Refs. [55,56], and [57].

A mesh sensitivity analysis is performed using several mesh sizes. Table 2 shows five cases regarding a number of the elements applied on the left half of the symmetric geometry, from normal up to extremely fine. Mean Nusselt number (Nu_{mean}) to the absolute sequential error, are two criteria to probe the appropriate grid size. The case in which absolute sequential error is less than 0.05 %, is the fourth one, extra fine mesh quality along with 24800 domain and boundary elements. Thus, case 4 can be selected to obtain all the results through it. Besides Table 2, We have depicted Fig. 2 to emphasize the chosen grid size, where the evaluation of the velocity components crossing the mid-plane of the double pipes space is considered. As seen, there have been some significant fractures in the curve with the largest elements (Case 1, Normal mesh quality). Next, the intensity of the fractures is diminished through the cases with the smaller elements; so that, cases 4 and 5 are so smooth, without any evident fractures. Hence, case 4 is utilized for obtaining the results in the present study. Fig. 3 show different views of the physical model via the chosen grid size (Case 4). A high density of the elements close to the inner and outer pipes is adopted. The zoomed views have also been provided to better understand the mentioned areas, where heat and fluid flow get more importance.

4. Computational code validation

To ensure that the present numerical code is applicable and there is no leakage in its body, We have provided two comparisons between the current code and the provided results in the most related papers in the literature. The first one is the experiment work of Guj et al. [58], is considered. They [58] have evaluated pure air fluid flow within a double cylinder space which could be arranged eccentrically or concentric than together. Anyway, to make a closer comparison, concentric arrangement is under consideration. About

Table 3
The predefined value and the range of dimensionless numbers and parameters specified in the results and discussion atmosphere.

Row	Parameters	Default values	Taken Range	
			Lower Bound	Upper Bound
1	n (Carreau index)	0.65	0.65	1.35
2	Ra (Rayleigh number)	10^5	10^4	10^6
3	R_K (Thermal conductivity Ratio)	100	1	100
4	φ_{NEPCM} (Nano- encapsulated phase change materials volume fraction)	0.025	5×10^{-3}	0.025
5	φ_{SNP} (Simple nanoparticles, Al_2O_3)	0.025	5×10^{-3}	0.025
6	θ_f (Fusion temperature)	0.3	0.1	0.7

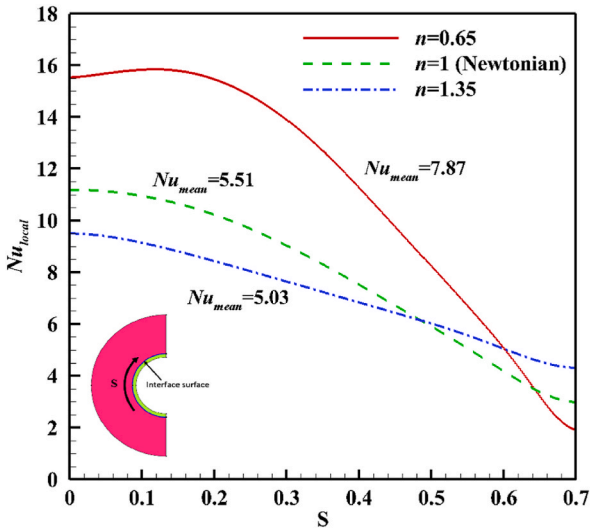

Fig. 6. Local Nusselt number (Nu_{local}) dependent on the different values of Carreau index (n).

the taken boundary conditions, it should be noted that the inner and outer cylinders were in the hot and cold temperatures, respectively. According to Fig. 4, the isotherm contours between the present code (left side), and Guj et al. [58] work (right side), have been compared. To do it, the equivalent Rayleigh number is accounted to be $Ra = 82700$. As seen, the patterns for the isotherm contours provided via the current code are completely in agreement with those obtained in Guj et al. [58] work.

The second comparison is related to one of our previous studies, Ghalambaz et al. [52], in which free convection heat transfer of MgO-MWCNTs/Ethylene Glycol as a Newtonian hybrid nanoliquid inside a star-shaped geometry has been simulated. In addition, the mentioned study [52] have covered the impressions of radiation mode and MHD on the heat and fluid flow. Importantly, the suggested boundary conditions are the same in both studies. Fig. 5 provide a comparison for streamlines in $Ra = 10^5$, and Pr = 155.3 in the absence of radiation and MHD effects. The obtained patterns in each figure are fully symmetric against the vertical axis. Besides, in the present study, versus the previous one [52], we have considered a uniform density for the depicted streamlines throughout the mentioned space. All in all, the compared streamlines in two studies, present and previous, show common patterns in the star shape geometry.

5. Results and discussion

Hereon, impressions of the introduced dimensionless numbers and parameters on the heat and fluid flow of NEPCM/Al_2O_3-Kerosene non-Newtonian hybrid nanoliquid placed inside the double pipes space are probed. Curves, contours as well as streamlines are the ways to reveal the obtained results.

At first, the predefined values and the taken range of the numbers and parameters have been determined in Table 3. It should be noted that all parameter values are assumed identical to those used in the mesh study. Any parameter value differing from the mesh study will be explicitly indicated.

Fig. 6 depicts the influence of the Carreau index (n) on the local Nusselt number. As seen, the obtained patterns for the three curves are generally the same, high and low values of the local Nusselt number on the below and top of the interface surface, respectively. The cold hybrid nanoliquid, firstly, meets the below areas of the hot inner pipe. It causes high gradients in the mentioned areas. As long as the fluid flows close to the interface surface, it absorbs the heat from the inner pipe, and the thermal equilibrium occurs, gradually. Nevertheless, thermal gradient intensity is diminished so that the minimum values are observed on the top of the inner pipe, where the most thermal equilibrium is established.

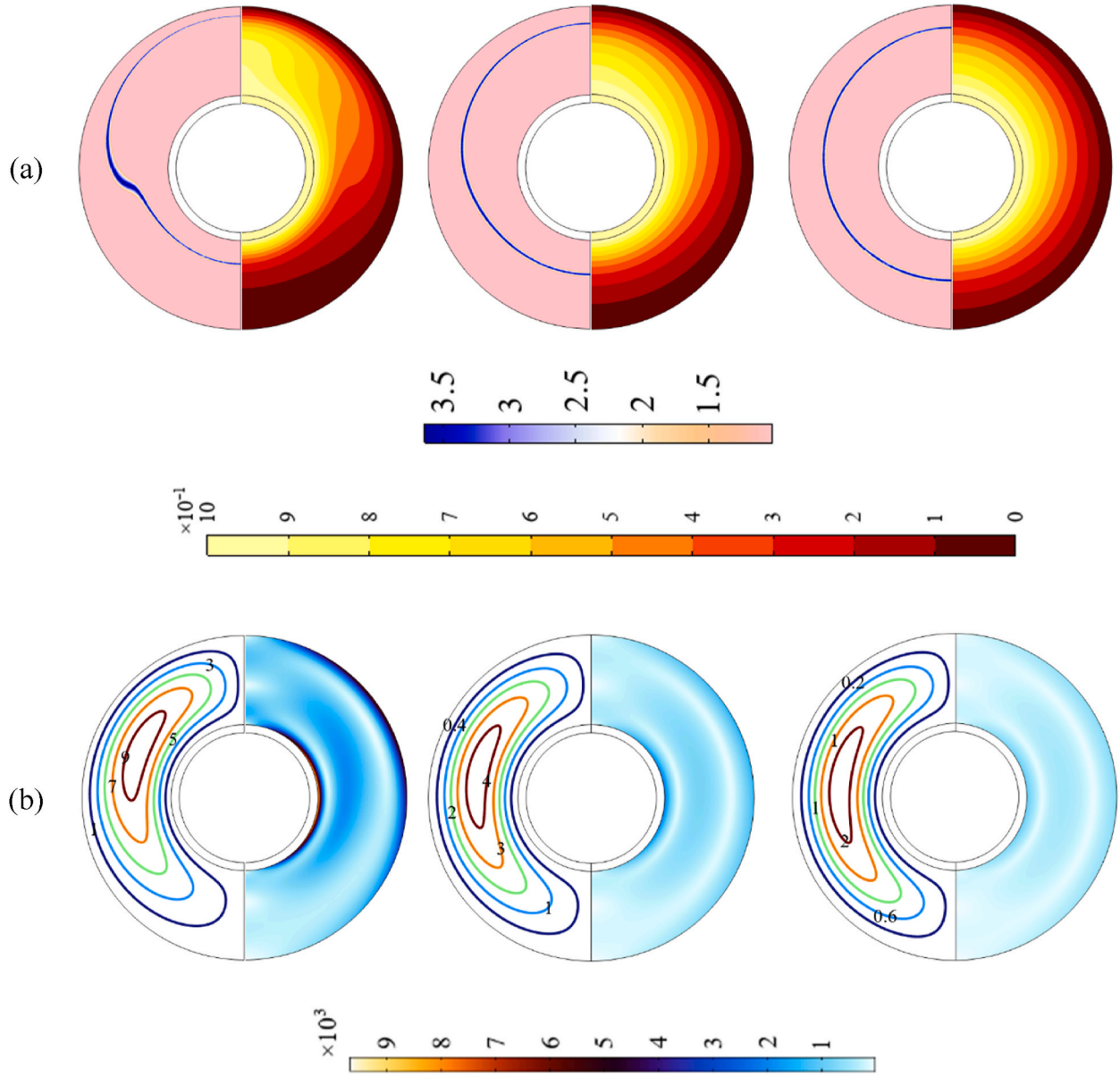

Fig. 7. Impression of Carreau index on the (first row) *Cr* parameter on the left half and isotherm contours on the right half, (second row) streamlines on the left half, and shear rate on the right half.

Changing the Carreau index (n) has an evident impression on the local Nusselt number. The curve regarding $n = 0.65$ has taken the lead, while, that $n = 1.35$ has the lowest value of Nusselt number. Unlike the Newtonian fluids, the non-Newtonian ones can behave as a shear thinning and/or a shear thickening fluid under the encountered stress. Based on the well-known principles of the Carreau model, when $n < 1$, the fluid finds the shear-thinning property. Although, $n > 1$ leads to the shear thickening non-Newtonian fluid. The shear-thinning fluid (here $n = 0.65$), becomes less viscous and flows lighter than a Newtonian fluid. So, the improvement percentage of the mean Nusselt number for the shear-thinning hybrid nanoliquid against the regular Newtonian fluid is about 42 %. In contrast, the shear thickening one (here $n = 1.35$) gets more viscous and flows heavier than a Newtonian fluid. Hence, not only the mean Nusselt number is not improved, but also, there has also been a deterioration in the heat transfer rate, by 9 %. Thus, the thermal equilibrium via a lighter fluid is lower than that of a heavier one. The shear thinning and the shear thickening non-Newtonian fluids would be faster and slower than the Newtonian fluid, respectively. Hence, the first spends less time in the vicinity of the inner pipe, while the second would remain beside the interface surface for more time. In other words, the convection mode through the shear thinning and the shear thickening fluids is augmented and deteriorated, respectively.

The effect of the Carreau index (n) on *Cr*-isotherm contours as well as streamlines-shear rate are depicted in the first and second rows of Fig. 7. Here, symmetric geometry along with the boundary conditions are utilized and half of the geometry shows one of the

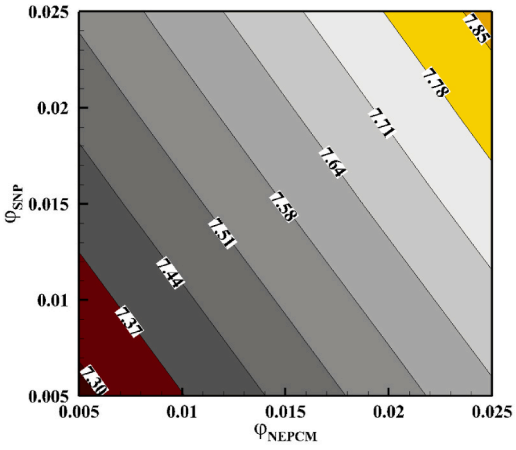

(a) n=0.65 (Shear thinning),

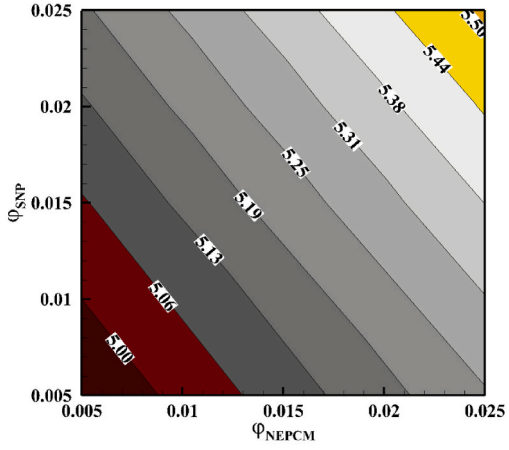

(b) n=1 (Newtonian),

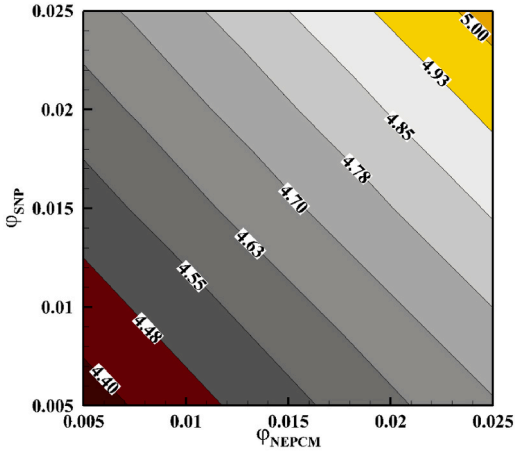

(c) n=1.35 (Shear thickening),

(caption on next page)

Fig. 8. Contours of mean Nusselt number (Nu_{mean}), dependent on the NEPCM concentration (φ_{NEPCM}) and simple nanoparticles concentration (φ_{SNP}), for (a) $n = 0.65$, (b) $n = 1$ (Newtonian), and (c) $n = 1.35$.

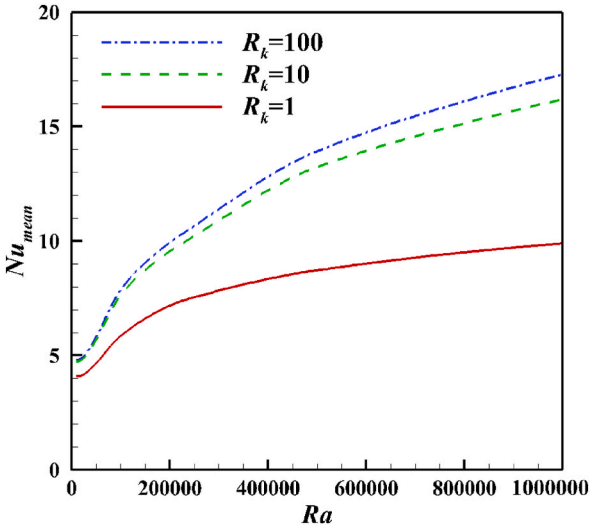

Fig. 9. Impression of Rayleigh number (Ra), and thermal conductivity ratio (R_k) on mean Nusselt number (Nu_{mean}).

mentioned results.

According to the first row, *Cr* contour is considered on the left-half. The right half shows the isotherm contours as well. The blue continuous ribbons that appeared in *Cr* contours, show a phase change process in the NEPCMs, where they are fully melted, and the heat absorption has been prevented. As a comprehensive rule, the obtained patterns for the ribbons obey the shape of the thermal gradients. When a shear thinning property is dominant, the thermal gradients would be flared up and tended to the above areas of the double pipes space. A fluid with a shear thickening property leads to the subsidence of the thermal gradients. Hence, the blue ribbon for $n = 0.65$ meets the upper areas of the double pipes space and misses its uniform thickness, where the melted NEPCMs become dense in the middle area of the double pipes space by the shape of the thermal gradient layer. On the other hand, the ribbon related to $n = 1.35$ has remained in the intermediate areas with a uniform thickness, in which the density of the melted NEPCMs is the same throughout the ribbon.

The left and right sides of the second row in Fig. 7 display the streamlines and shear rates for three different values of the Carreau index (n), respectively. These streamlines allow for a comparison between the shear-thinning and shear-thickening hybrid nanoliquids. A shear-thinning fluid, with $n = 0.65$, results in a lighter liquid, whereas a heavier liquid is observed in the shear-thickening fluid with $n = 1.35$. Thus, the lighter shear thinning fluid shows more pronounced streamlines and higher velocity compared to the heavier shear thickening fluid.

The shear rate occurred through each one of the Carreau index (n) values has a maximum amount close to the inner and outer pipe surface. The shear rate effect on the fluid with shear thinning property ($n = 0.65$) is significant. However, the shear thickening fluid ($n = 1.35$) does not have any evident reaction to the applied shear rate. Unlike the shear thickening hybrid nanoliquid ($n = 1.35$), which is resistant to the encountered shear stress because of its high viscosity and low velocity, the non-Newtonian hybrid nanoliquid with low viscosity ($n = 0.65$) and high velocity has an extreme shear rate on the preferred surfaces. Hence, it can be emphasized that the intensity of the shear rate is a function of the fluid velocity in agreement with the related mathematical equations. In conclusion, since the shear-thinning fluids can easily be moved, using them in the free convection heat transfer applications is suggested. Instead, the shear-thickening fluids have damping stress properties and can be utilized in other related applications.

The contour of the mean Nusselt number as a function of the volume fraction of simple nanoparticles (vertical axis) and NEPCM (horizontal) has been evaluated in Fig. 8. The results are provided for the three mentioned values of the Carreau index (n), separately. The main purpose is that the various values of mean Nusselt number for NEPCM-Al_2O_3-Kerosene as Newtonian and non-Newtonian hybrid nanoliquid to be accessed without any limitation about simulation and so on. As seen, the range of mean Nusselt number via shear thinning hybrid nanoliquid is more than Newtonian, and Newtonian is more than shear thickening hybrid nanoliquid. With a focus on each contour set, it can be found that the highest value of the mean Nusselt number has been provided through a 0.025 % volume fraction of each one of simple nanoparticles, and NEPCMs. In contrast, the lowest value of the mean Nusselt number is provided when the minimum portion of two types of nanoparticles have been dispersed in the host fluid. The distribution of the nanoparticles in the host fluid increases the thermal conductivity of the obtained synthesis. Hence, more presence of the nanoparticles augments the mean Nusselt number. Interestingly, the improvement percentage in each type of fluid, shear thinning, Newtonian, and shear thickening is calculated as 7.5 %, 10 %, and over 13.5 %, respectively. Indeed, increasing the thermal conductivity via more presence of the nanoparticles is firstly effective on the shear thickening hybrid nanoliquid, secondly, Newtonian hybrid nanoliquid, and finally, shear

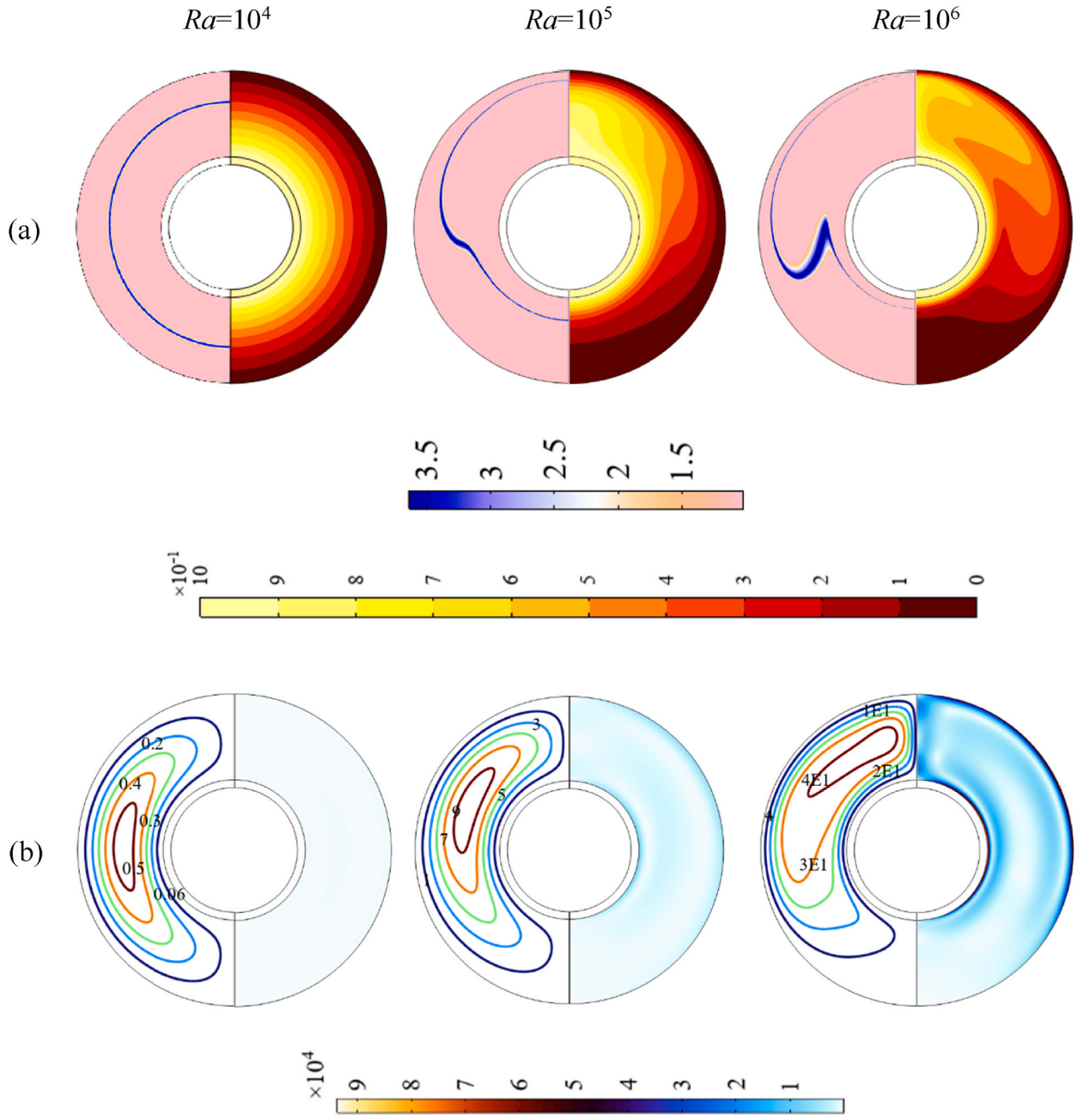

Fig. 10. Impression of Rayleigh number (*Ra*) on the (first row) *Cr* on the left-half and isotherm contours on the right-half, (second row) streamlines on the left-half and shear rate on the right half.

thinning hybrid nanoliquid. When the nanoparticles are appended to the host fluid, both viscosity and thermal conductivity are increased. The shear-thickening hybrid nanoliquid has already high viscosity. Thus, adding the nanoparticles cannot bring significant impression on the overall viscosity of the fluid. So, increasing the thermal conductivity can be quite beneficial in such fluids. In contrast, shear thinning fluid with its low viscosity reacts to increasing both viscosity and thermal conductivity. Since a significant increment of the viscosity is a negative factor in the nanoliquid field, the improvement percentage of the mean Nusselt number in the shear thinning fluid is less than one provided via the shear thickening fluid.

Fig. 9 shows the evaluation of the Mean Nusselt number affected by both of thermal conductivity ratio (R_k), and Rayleigh number (*Ra*). The first raises of conduction mode, while the second shows the power of the convection mode. Indeed, conduction and convection modes make up conjugate heat transfer between the double pipes space. The high value of Rayleigh number (*Ra*) causes convection mode to have a major portion in that space. Instead, raising of thermal conductivity ratio (R_k) means that the conduction

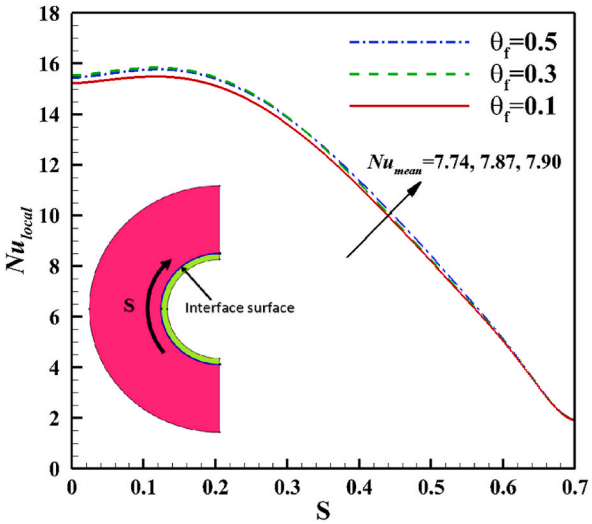

Fig. 11. Local Nusselt Number (Nu_{local}) in the different values of fusion temperature (θ_f).

mode is the governed one into the considered space. According to the obtained results in Fig. 9, when the convection mode is weak, increasing the thermal conductivity ratio (R_k) has a minor positive impression on the mean Nusselt number. On the other hand, in case of conduction mode is feeble, raising of Rayleigh number (Ra) augments the heat transfer rate, slightly. In contrast, whenever one of the mentioned modes is strong, increasing the other has an impressive positive effect on the mean Nusselt number. It is because of a synergistic interaction phenomenon between both conduction and convection modes, which creates a robust conjugate heat transfer within the double pipes space. A powerful conduction mode can be formed by choosing a high thermal conductivity material for the inner pipe body. In addition, improvement of the buoyancy forces via a high Rayleigh number (Ra) makes a strong convection mode. Nevertheless, defect in each mode deteriorates conjugate heat transfer within the double pipes space. Overall, the highest value of the mean Nusselt number is reached, over $Nu_{mean}>17$, via the highest values of both of thermal conductivity ratio (R_k) and Rayleigh number (Ra). It is about 2 times larger than the mean Nusselt number in the default state defined in the present study.

The effect of various values of Rayleigh number (Ra), 10^4, 10^5, and 10^6, on Cr-isotherm contours has been shown in the first row of Fig. 10. As referred, increasing Rayleigh number (Ra) causes buoyancy forces to be augmented. An enhanced fluid flow leads to stronger thermal gradients throughout the double pipes space. Hence, by increasing Rayleigh number (Ra), isotherm contours have impressively flared up. Since Cr contours comply with isotherm patterns, when Rayleigh number (Ra) is increased, the blue ribbon which shows melting NEPCMs has gotten a sharp shape, gradually. In addition, the thickness of the blue ribbon would not be uniform anymore; On the other hand, the melting NEPCMs in the middle region of the double pipes space would be dense. As a defined rule in the present study, the second row in Fig. 10 depicts streamlines and shear rates as well. Hereon, the impact of Rayleigh number (Ra) on both of them is evaluated. When convection mode via increasing Rayleigh number (Ra) is dominant, NEPCM/Al2O3-Kerosene non-Newtonian hybrid nanoliquid will have a higher velocity in the mentioned space. Hence, the streamlines created via high values of the Rayleigh number (Ra) are much stronger than those obtained in the low values of the Rayleigh number (Ra). Buoyancy forces have a direct impact on the overall shear rate that appears in the double pipes space. The weak streamlines lead to an insignificant shear rate. Instead, the powerful streamlines provide a violent shear rate throughout the space.

The last part of the result and discussion section has been assigned to the evaluation of the fusion temperature (θ_f) effect on the non-Newtonian hybrid nanoliquid. Fig. 11 depicts the local Nusselt number for three different values of fusion temperature, $\theta_f = 0.1$, 0.3, and 0.5. As seen, variations of the mentioned parameter cannot create any special change in the local Nusselt number value. It is important to note that the NEPCMs get phase change without any significant temperature difference. Indeed, the phase change process which includes heat absorption, majorly occurred under the latent heat transfer mode. However, the obtained thermal gradients are affected by the sensible aspect of the heat transfer. Hence, the changes observed in Fig. 12 through increasing or decreasing fusion temperature are so slight.

Fig. 12 reveals Cr-isotherm contours, the first row, and streamlines-shear rate, the second row, for the three adopted values of fusion temperature. Apart from Cr contours, three other ones do have not any evident variation. As referred, it is because of the occurring phase-changing process of the NEPCMs under the latent heat transfer mode; while, isotherm contours, streamlines, and shear rates, all of them, obey the sensible heat transfer mode. Anyway, when the fusion temperature is increased, the melting NEPCMs are placed near the hot inner pipe. Instead, decreasing the fusion temperature, causes the NEPCMs to get melt away from the hot inner pipe. A high value of fusion temperature means that the NEPCMs melt at a higher temperature, and hence, the blue ribbon appears close to the hot inner pipe. However, a low value of θ_f, holds the phase change process, nearer to the cold outer pipe, without any additional heat for the melting process.

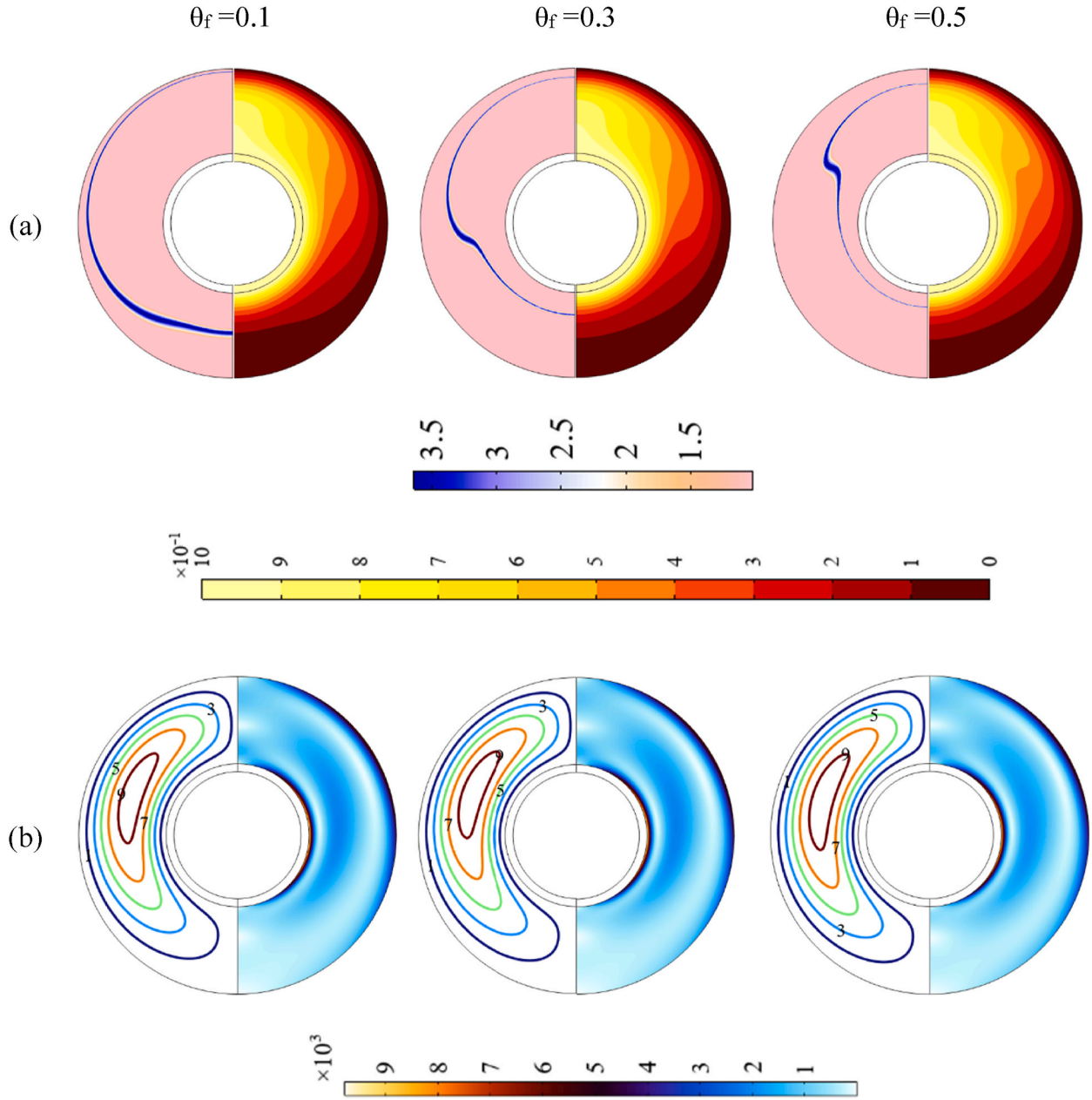

Fig. 12. Impression of fusion temperature (θ_f) on the (First row) *Cr* on the left half and isotherm contours on the right half, (Second row) streamlines on the left half, and shear rate on the right half.

6. Conclusion

Our attempt in the present study was to understand the non-Newtonian behavior of NEPCMs- Al_2O_3/Kerosene within a double pipes space. After creating a computational code and checking it with the results provided in the other valid papers, the results have been extracted in accordance with the dimensionless numbers and parameters. Thus, the most important ones collected and described as follows.

I. The hybrid nanoliquid with shear thinning properties is suitable for free convection heat transfer applications. The heat transfer augmentation and deterioration percentage via the shear thinning and shear thickening hybrid nanoliquid against the Newtonian one is about 42 % and 9 %, respectively. Shear thinning hybrid nanoliquid is lighter than the two other types; hence, easier circulation is provided as well. Instead, shear thickening hybrid nanoliquid is heavier than the others; consequently, circulation through the mentioned liquid would be hard.

II. Increasing the concentration of NEPCMs and simple nanoparticles is always beneficial and improves heat transfer. influence on the heat transfer rate. The shear-thickening hybrid nanoliquid is more affected by appending the nanoparticles in the host fluid, so the heat transfer improvement percentage is by 13.5 %; However, the shear-thinning hybrid nanoliquid due to its low value of dynamic viscosity shows less sensitivity to adding the both of nanoparticles. The heat transfer improvement percentage is just 7.5 % through $n = 0.65$.
III. Simultaneous increasing of Rayleigh number (Ra), and thermal conductivity ratio (R_k) enhances heat transfer rate, impressively. Importantly, if, one of them gets weak, the effect of the other on the heat transfer rate cannot be significant. Based on the maximum values for Rayleigh number (Ra), and thermal conductivity ratio (R_k), which are taken in the current study, the mean Nusselt number reaches the value about 2 times more than its value in the default state. Via an astounding conjugate heat transfer, the isotherm and Cr contours are flared up.
IV. Changing the fusion temperature notably changes the location of the phase transition region. The Cr phase change region, which appears as a blue ribbon in Cr contours, gets close to the inner hot pipe as the fusion temperature increases.

CRediT authorship contribution statement

Mohamed Bouzidi: Methodology, Formal analysis, Conceptualization. **Hakim S. Sultan Aljibori:** Investigation. **Zehba Raizah:** Formal analysis. **Mohammed Hasan Ali:** Software, Data curation. **Taoufik Saidani:** Methodology, Formal analysis. **Faisal Alresheedi:** Writing – original draft, Investigation. **Ahmed Elhassanein:** Writing – review & editing, Conceptualization. **Mahmoud Sabour:** Software, Methodology, Formal analysis, Conceptualization. **Mohammad Ghalambaz:** Writing – review & editing, Validation, Supervision.

Declaration of competing interest

The authors clarify that there is no conflict of interest for report.

Acknowledgements

The authors are thankful to the Deanship of Graduate Studies and Scientific Research at University of Bisha for supporting this work through the Fast-Track Research Support Program. The authors extend their appreciation to the Deanship of Research and Graduate Studies at King Khalid University for funding this work through large Research Group Project under the grant number (RGP2/198/45). The authors extend their appreciation to the Deanship of Scientific Research at Northern Border University, Arar, KSA for funding this research work through the project number "NBU-FPEJ-2025-2225-05".

Data availability

Data will be made available on request.

References

[1] E.Y. Rios-Iribe, M.E. Cervantes-Gaxiola, E. Rubio-Castro, O.M. Hernández-Calderón, Heat transfer analysis of a Non-Newtonian fluid flowing through a plate heat exchanger using CFD, Appl. Therm. Eng. 101 (2016) 262–272.
[2] N. Kushwaha, T.C. Kumawat, K.D.P. Nigam, V. Kumar, Heat transfer and fluid flow characteristics for newtonian and non-Newtonian fluids in a tube-in-tube helical coil heat exchanger, Ind. Eng. Chem. Res. 59 (9) (2020) 3972–3984.
[3] J.C. Gabelle, F. Augier, A. Carvalho, R. Rousset, J. Morchain, Effect of tank size on kLa and mixing time in aerated stirred reactors with non-newtonian fluids, Can. J. Chem. Eng. 89 (5) (2011) 1139–1153.
[4] R. Fijan, M. Basile, R. Lapasin, S. Šostar-Turk, Rheological properties of printing pastes and their influence on quality-determining parameters in screen printing of cotton with reactive dyes using recycled polysaccharide thickeners, Carbohydr. Polym. 78 (1) (2009) 25–35.
[5] L. Bin, Study on Modified Viscous Fluid and Its Damper, Southeast University, 2007.
[6] I. Pishkar, B. Ghasemi, A. Raisi, S.M. Aminossadati, Numerical study of unsteady natural convection heat transfer of newtonian and non-Newtonian fluids in a square enclosure under oscillating heat flux, J. Therm. Anal. Calorim. 138 (2019) 1697–1710.
[7] K. Yazdani, M. Sahebjamei, A. Ahmadpour, Natural convection heat transfer and entropy generation in a porous trapezoidal enclosure saturated with power-law Non-Newtonian fluids, Heat Transf. Eng. 41 (11) (2019) 982–1001.
[8] A. Jahanbakhshi, A.A. Nadooshan, M. Bayareh, Magnetic field effects on natural convection flow of a Non-Newtonian fluid in an L-shaped enclosure, J. Therm. Anal. Calorim. 133 (2018) 1407–1416.
[9] P.P. Roy, S. Chowdhury, M.H. Raj, M.Q. Islam, S. Saha, Forced, natural and mixed convection of non-newtonian fluid flows in a square chamber with moving lid and discrete bottom heating, Results in Engineering 17 (2023) 100939.
[10] D.S. Loenko, M.A. Sheremet, Mathematical modeling of pseudoplastic nanofluid natural convection in a cavity with a heat-generating unit and solid finned heat sink, Mathematics 11 (18) (2023) 3868.
[11] O. Benhizia, M. Bouzit, Natural convection of Non- newtonian dilatant fluid in the gap between an outer cylinder and inner cylinder with grooves, Heat Tran. Res. 55 (8) (2024).
[12] I.S. Chuhan, J. Li, M.S. Ahmed, I. Samuilik, M.A. Aslam, M.A. Manan, Numerical investigation of double-diffusive convection in an irregular porous cavity subjected to inclined magnetic field using finite element method, Mathematics 12 (6) (2024) 808.
[13] B. Farhat, N. Kaid, S. Alqahtani, Y. Menni, B.M. Alshammari, L. Kolsi, Finite element analysis of laminar natural convection in a differentially heated porous cavity using the darcy–brinkman model, Processes 12 (9) (2024) 1974.
[14] L. Kolsi, F. Selimefendigil, M. Omri, H. Rmili, B. Ayadi, C. Maatki, B.M. Alshammari, CFD study of MHD and elastic wall effects on the nanofluid convection inside a ventilated cavity including perforated porous object, Mathematics 11 (3) (2023) 695.

[15] O. Younis, S.E. Ahmed, A. Abderrahmane, A. Alenazi, A.M. Hassan, Hydrothermal mixed convection in a split-lid-driven triangular cavity suspended by NEPCM, Mathematics 11 (6) (2023) 1323.
[16] A.H. Majeed, R. Mahmood, D. Liu, Y. Zhang, J.Y. Zhang, H.Y. Ren, A.S. Hendy, M.R. Ali, Effects of oscillation on convective thermal flow in a vertical enclosure filled by nanofluid particles, Case Stud. Therm. Eng. 61 (2024) 105133.
[17] M. Tasmin, P. Nag, Z.T. Hoque, M.M. Molla, Non-newtonian effect on heat transfer and entropy generation of natural convection nanofluid flow inside a vertical wavy porous cavity, SN Appl. Sci. 3 (2021) 1–29.
[18] M. Hojjat, S.G. Etemad, R. Bagheri, J. Thibault, Convective heat transfer of Non-Newtonian nanofluids through a uniformly heated circular tube, Int. J. Therm. Sci. 50 (4) (2011) 525–531.
[19] Y. Tan, Z. He, T. Xu, X. Fang, X. Gao, Z. Zhang, Experimental investigation of heat transfer and pressure drop characteristics of Non-Newtonian nanofluids flowing in the shell-side of a helical baffle heat exchanger with low-finned tubes, Heat Mass Tran. 53 (2017) 2813–2827.
[20] A. Abderrahmane, M. Hatami, M. Medebber, S. Haroun, S.E. Ahmed, S. Mohammed, Non-newtonian nanofluid natural convective heat transfer in an inclined half-annulus porous enclosure using FEM, Alex. Eng. J. 61 (7) (2022) 5441–5453.
[21] B.A.K. Naik, A.V. Vinod, Heat transfer enhancement using Non-Newtonian nanofluids in a shell and helical coil heat exchanger, Exp. Therm. Fluid Sci. 90 (2018) 132–142.
[22] B.A.K. Naik, A.V. Vinod, Natural convection heat transfer in a shell and helical coil heat exchanger using Non-Newtonian nanofluids, De Gruyter 15 (2) (2020) 20190058.
[23] S. Anitha, M. Pichumani, Numerical analysis on heat transfer performance of industrial double-tube heat exchanger using CNT: newtonian/Non-newtonian hybrid nanofluids, J. Therm. Anal. Calorim. 147 (17) (2022) 9603–9624.
[24] A. Vallabh, P. Ghoshdastidar, Numerical simulation of heat transfer in laminar natural convection of mixed newtonian-non-newtonian and pure non-newtonian nanofluids in a square enclosure, J. Therm. Sci. Eng. Appl. 13 (6) (2021) 061008.
[25] H. Maleki, M.R. Safaei, A.A. Alrashed, A. Kasaeian, Flow and heat transfer in Non-Newtonian nanofluids over porous surfaces, J. Therm. Anal. Calorim. 135 (2019) 1655–1666.
[26] A. Shahsavar, M.A. Bakhshizadeh, M. Arici, M. Afrand, S. Rostami, Numerical study of the possibility of improving the hydrothermal performance of an elliptical double-pipe heat exchanger through the simultaneous use of twisted tubes and Non-Newtonian nanofluid, J. Therm. Anal. Calorim. 143 (3) (2021) 2825–2840.
[27] H. Waqas, M.J. Hasan, C. Ji, D. Liu, C. Kang, T. Muhammad, Melting performance of PCM with MoS2 and Fe3O4 nanoparticles using leaf-based fins with different orientations in a shell and tube-based TES system, Int. Commun. Heat Mass Tran. 158 (2024) 107944.
[28] A. Hafeez, D. Liu, A. Khalid, M. Du, Melting heat transfer features in a bö dewadt flow of hybrid nanofluid (cu− Al2O3/water) by a stretching stationary disk, Case Stud. Therm. Eng. 59 (2024) 104554.
[29] H. Waqas, M. Hussain, S. Ahmad, Q.M. Al-Mdallal, M.A. Abdelmohimen, Enhancing thermal storage performance: a combined approach using nano-integrated phase change material and arc fins, Int. Commun. Heat Mass Tran. 161 (2025) 108549.
[30] F.H. Ali, H.K. Hamzah, S.Y. Ahmed, M.A. Ismael, Z. Haddad, M. Ghalambaz, A.M. Abed, K. Al-Farhany, W. Jamshed, M.R. Eid, Convective heat transference of Non-Newtonian functional phase variation nano-encapsulated liquids, Int. J. Mod. Phys. B 37 (29) (2023) 2350258.
[31] A. Dogonchi, N. Bondareva, M. Sheremet, S. El-Sapa, A.J. Chamkha, N.A. Shah, Entropy generation and heat transfer performance analysis of a Non-Newtonian NEPCM in an inclined chamber with complicated heater inside, J. Energy Storage 72 (2023) 108745.
[32] S. Hussain, T. Tayebi, T. Armaghani, A. Rashad, H. Nabwey, Conjugate natural convection of Non-Newtonian hybrid nanofluid in wavy-shaped enclosure, Appl. Math. Mech. 43 (3) (2022) 447–466.
[33] S. Ahmad, D. Liu, H. Waqas, S. Munir, Numerical simulation of magnetohydrodynamics double-diffusive natural convection in a cavity with non-uniform heated walls, Appl. Therm. Eng. 253 (2024) 123778.
[34] S. Batool, M. Nawaz, Investigation of thermal enhancement in Non-Newtonian fluid with hybrid micro-structures in an enclosure, Int. Commun. Heat Mass Tran. 117 (2020) 104777.
[35] M. Bahiraei, A. Godini, A. Shahsavar, Thermal and hydraulic characteristics of a minichannel heat exchanger operated with a Non-Newtonian hybrid nanofluid, J. Taiwan Inst. Chem. Eng. 84 (2018) 149–161.
[36] A.A. Nadooshan, H. Eshgarf, M. Afrand, Measuring the viscosity of Fe3O4-MWCNTs/EG hybrid nanofluid for evaluation of thermal efficiency: newtonian and non-Newtonian behavior, J. Mol. Liq. 253 (2018) 169–177.
[37] A. Shahsavar, M. Bahiraei, Experimental investigation and modeling of thermal conductivity and viscosity for Non-Newtonian hybrid nanofluid containing coated CNT/Fe3O4 nanoparticles, Powder Technol. 318 (2017) 441–450.
[38] M. Bahiraei, M. Berahmand, A. Shahsavar, Irreversibility analysis for flow of a Non-Newtonian hybrid nanofluid containing coated CNT/Fe3O4 nanoparticles in a minichannel heat exchanger, Appl. Therm. Eng. 125 (2017) 1083–1093.
[39] A.A. Alnaqi, J. Alsarraf, A.A. Al-Rashed, M. Afrand, Thermal-hydraulic analysis and irreversibility of the MWCNTs-SiO2/EG-H2O Non-Newtonian hybrid nanofluids inside a zigzag micro-channels heat sink, Int. Commun. Heat Mass Tran. 122 (2021) 105158.
[40] A. Dawar, S. Islam, A. Alshehri, E. Bonyah, Z. Shah, Heat transfer analysis of the MHD stagnation point flow of a Non-Newtonian tangent hyperbolic hybrid nanofluid past a non-isothermal flat plate with thermal radiation effect, J. Nanomater. 2022 (2022) 1–12.
[41] S. Barlak, O.N. Sara, A. Karaipekli, S. Yapıcı, Thermal conductivity and viscosity of nanofluids having nanoencapsulated phase change material, Nanoscale Microscale Thermophys. Eng. 20 (2) (2016) 85–96.
[42] D. Pau, C. Fleischmann, M. Spearpoint, K. Li, Thermophysical properties of polyurethane foams and their melts, Fire Mater. 38 (4) (2014) 433–450.
[43] G. Venkatesan, G.-P. Jin, M.-C. Chyu, J.-X. Zheng, T.-Y. Chu, Measurement of thermophysical properties of polyurethane foam insulation during transient heating, Int. J. Therm. Sci. 40 (2) (2001) 133–144.
[44] S. Ceramaret, Physical, mechanical, thermal, electrical and chemical properties, in: Bôle, 2013 available at: http://archive.is/0Brd9.
[45] D.K. Agarwal, A. Vaidyanathan, S.S. Kumar, Synthesis and characterization of kerosene–alumina nanofluids, Appl. Therm. Eng. 60 (1–2) (2013) 275–284.
[46] H. Sardar, M. Khan, Mixed convection flow and heat transfer mechanism for Non-Newtonian carreau nanofluids under the effect of infinite shear rate viscosity, Physica Scripta 95 (3) (2020) 035225.
[47] R. Bird, Armstrong, O. Hassager, Dynamics of Polymeric Liquids, Wiley, 1977.
[48] S. Kuravi, K.M. Kota, J. Du, L.C. Chow, Numerical investigation of flow and heat transfer performance of nano-encapsulated phase change material slurry in microchannels 131 (6) (2009) 062901.
[49] K. Kahveci, Buoyancy Driven Heat Transfer of Nanofluids in a Tilted Enclosure, 2010 062501.
[50] S.H. Zadeh, M. Sabour, S. Sazgara, M. Ghalambaz, Free convection flow and heat transfer of nanofluids in a cavity with conjugate solid triangular blocks: employing Buongiorno's mathematical model, Phys. Stat. Mech. Appl. 538 (2020) 122826.
[51] J.R. Babu, K.K. Kumar, S.S. Rao, State-of-art review on hybrid nanofluids, Renew. Sustain. Energy Rev. 77 (2017) 551–565.
[52] M. Ghalambaz, M. Sabour, I. Pop, D. Wen, Free convection heat transfer of MgO-MWCNTs/EG hybrid nanofluid in a porous complex shaped cavity with MHD and thermal radiation effects, Int. J. Numer. Methods Heat Fluid Flow 29 (11) (2019) 4349–4376.
[53] A.A. Sakhir Abed, Numerical simulation of laminar incompressible driven cavity flow in a l-shape domain, Int. J. Mech. Eng. Technol. 10 (1) (2019) 119–132.
[54] S. Mehryan, M. Ghalambaz, L.S. Gargari, A. Hajjar, M. Sheremet, Natural convection flow of a suspension containing nano-encapsulated phase change particles in an eccentric annulus, J. Energy Storage 28 (2020) 101236.
[55] T. Basak, S. Roy, A. Balakrishnan, Effects of thermal boundary conditions on natural convection flows within a square cavity, Int. J. Heat Mass Tran. 49 (23–24) (2006) 4525–4535.
[56] M.h. Souli, D.J. Benson, Arbitrary Lagrangian Eulerian and fluid-structure Interaction: Numerical Simulation, John Wiley & Sons, 2013.
[57] R. Codina, G. Houzeaux, H. Coppola-Owen, J. Baiges, The fixed-mesh ALE approach for the numerical approximation of flows in moving domains, J. Comput. Phys. 228 (5) (2009) 1591–1611.
[58] G. Guj, S. Iannetta, G. Moretti, Experimental analysis of thermal fields in horizontally eccentric cylindrical annuli, Exp. Fluid 12 (1992) 385–393.